Journal of Materials Chemistry A

PAPER

View Article Online
View Journal | View Issue

Cite this: J. Mater. Chem. A, 2015, 3, 9510

Engineering hollow mesoporous silica nanocontainers with molecular switches for continuous self-healing anticorrosion coating†

Tao Chen,[ab] Renpeng Chen,[a] Zhong Jin*[a] and Jie Liu*[ac]

Received 12th February 2015
Accepted 20th March 2015

DOI: 10.1039/c5ta01188d

www.rsc.org/MaterialsA

Here we report a new light-responsive and self-healing anticorrosion coating by incorporating hollow nanocontainers with smart molecular switches. The smart coating was obtained by immobilizing photoresponsive azobenzene molecular switches in the nanopores of hollow mesoporous silica nanocontainers. These novel nanocontainers with hollow cavities can encapsulate active molecules under visible light and release them under ultraviolet irradiation. The release of benzotriazole from the hollow nanocontainers can be started and stopped with high controllability, which provides an effective approach to avoid excessive release of active molecules after corrosion healing. The results of scanning vibrating electrode technique demonstrate that the azobenzene molecular switch modified hollow mesoporous silica nanocontainers exhibit excellent continuous photosensitive self-healing performance for improving the long-term performance of aluminium alloy.

Introduction

Metal corrosion is a world-wide serious issue causing enormous economic losses to the aerospace, automotive and petroleum industries. For example, the aluminium alloy AA2024, as a very important material, is broadly used in the aircraft industry due to its excellent weight-to-strength ratio. Unfortunately, intermetallic inclusions of this alloy make it peculiarly prone to localized pitting corrosion.[1] The use of chromate conversion coating is a relatively effective method to protect the underlying metal from corrosion.[2] However, there are concerns regarding the known toxic, carcinogenic and pollutive nature of hexavalent chromium.[3] It is highly desirable to develop self-healing anticorrosion coatings to take the place of hexavalent chromium for corrosion protection. The addition of stimuli-responsive nanocontainers encapsulating corrosion inhibitors to passive coating is a feasible way to continuously protect the underlying metal substrates. Such smart nanocontainers can control the release of encapsulated corrosion inhibitors under the stimulation of environmental changes, such as pH,[4] temperature,[5] light,[6] redox[7] and aggressive ionic strength.[8] The development of various stimuli-responsive nanocontainers with controlled uptake and release properties, high loading capacity, and structure stability offers a large number of promising designs for self-healing anticorrosion coatings.

Compared to other stimuli, such as pH or temperature, nanocontainers that respond to light stimulation can be operated more accurately and predictably. Light-sensitive nanocontainers for the capture and release of active molecules have been investigated in the field of drug delivery[9] and self-healing anticorrosion coatings.[6] For instance, silver nanoparticles were deposited into the polyelectrolyte shells of mesoporous titania and silica as light absorption centers, to remotely control the release of encapsulated corrosion inhibitors with high spatial and temporal accuracy, thus resulting in termination of the corrosion process.[6] It is worth mentioning that the periodic illumination of daylight can ensure the timely cure of unexpected scratches or other defects without further inspection. However, the development of light-sensitive nanocontainers incorporated into passive coatings for effective self-healing anticorrosion protection still remains a great challenge.

Azobenzene (Azo) is one of the most well-known photochromic molecules owing to its robustness, as well as rapid and reversible photo-isomerization between its *trans* and *cis* isomers.[10] Specifically, azobenzene and its derivations undergo reversible *trans–cis* isomerization upon exposure to light of the appropriate wavelength, which alters the distance between the two end para carbon atoms from 9 Å in the *trans* form to 5.5 Å in the *cis* form.[10b] The decrease in the size of *trans* to *cis* isomers in the pore interiors of mesoporous silica was exploited to regulate the entrance and egress of anticancer drugs.[11]

In this study, we reported a novel and facile light-triggered release system for an anticorrosion coating based on

[a]Key Laboratory of Mesoscopic Chemistry of MOE, School of Chemistry and Chemical Engineering, Nanjing University, Nanjing 210093, China. E-mail: zhongjin@nju.edu.cn; Tel: +86-25-83686220

[b]School of Chemical Engineering, Nanjing University of Science and Technology, Nanjing 210094, China

[c]Department of Chemistry, Duke University, Durham, USA. E-mail: j.liu@duke.edu

† Electronic supplementary information (ESI) available. See DOI: 10.1039/c5ta01188d

implanting azobenzene moieties into the nanopores of hollow mesoporous silica nanocontainers (HMSs). The nanocontainers not only possess a high loading capacity but can also control the entrance and release of trapped active molecules based on the dynamic motion of azobenzene molecules (Scheme 1). A water-born alkyd coating is employed in this work, which can provide excellent dispersibility for azobenzene-modified HMSs (Azo-HMSs). The Azo-HMSs were directly dispersed into the alkyd coating and then deposited on the surface of the aluminium plate. Upon ultraviolet (UV) irradiation, isomerization of azobenzene impeller from the thermodynamically stable *trans* isomer to the metastable *cis* isomer results in the opening of nanochannels, simultaneously expelling molecules out of the nanocontainers. Thereby, the corrosion inhibitors will be transported from the nanocontainers to corrosion sites so as to prevent the diffusion of anticorrosion agents and protect the underlying metal from severe damage. Exposure to visible light illumination has a reverse effect because the *cis* isomer of the azobenzene impeller transforms into the *trans* isomer. In this way, the residual corrosion inhibitors will not be sequentially released/wasted but can still be encapsulated within the nanocontainers to prevent the next corrosion. This is the first time that this reversible light-responsive release system was applied in the field of self-healing anticorrosion coatings. The fact that the reversible molecular switches can be opened and closed at will make this method rather flexible, providing the possibility of avoiding excess release of corrosion inhibitors after repairing the corrosion area. In addition, the operation of the azobenzene impeller in water also opens a new avenue for application in the area of intelligent remotely controlled corrosion protection coatings.

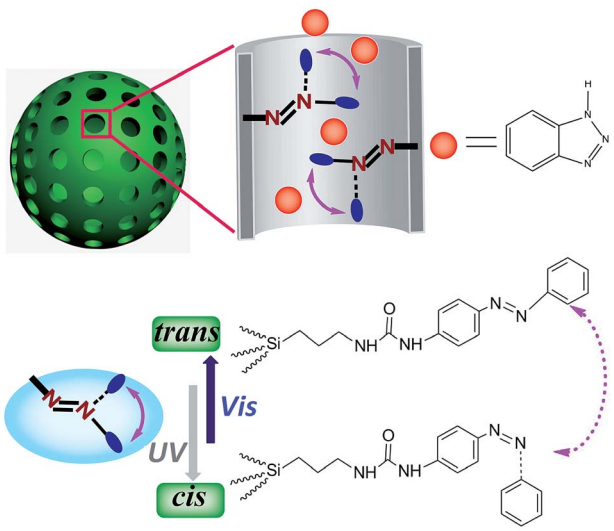

Scheme 1 Schematic of reversible release system by utilizing *trans–cis* photoisomerization of azobenzene molecules grafted in the mesopores of HMSs. UV irradiation at 365 nm converts azobenzene to the *cis* form, resulting in pore opening. The *cis* isomer of the azobenzene molecules transforms into the *trans* isomer under visible-light irradiation (450 nm), leading to pore closing.

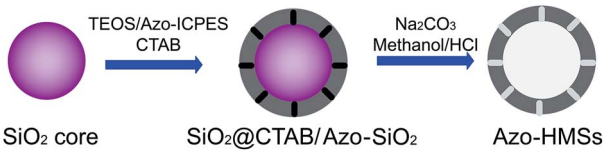

Scheme 2 Schematic diagram of the synthetic procedure of Azo-HMSs.

Experimental section

Materials

Thin films of aluminium alloy AA2024 of dimensions 1 cm × 4 cm × 0.04 cm were provided by XuSheng Co., (Nanjing, China). Tetraethylorthosilicate (TEOS), *N*-cetyltrimethylammonium bromide (CTAB), 4-phenylazoaniline (4-PAA) and isocyanatopropyltriethoxysilane (ICPES) were purchased from Sigma-Aldrich. Ammonia solution (25–28%) and sodium carbonate were obtained from Sinopharm Chemical Reagent Co., Ltd. All the solutions were prepared using deionized (DI) water (18.2 MΩ cm) originating from a Millipore Milli-Q water purification system.

Synthesis of SiO_2 nanoparticles

SiO_2 nanoparticles were synthesized following a previous report.[12] TEOS (2.5 mL) was rapidly added into a mixture solution of ethanol (107 mL), deionized water (2.5 mL) and ammonium hydroxide (2.5 mL). The mixture was then gently stirred at 30 °C for 2 h and a white silica colloidal suspension was formed. The SiO_2 nanoparticles were centrifugally isolated from the suspension and rinsed with ethanol and deionized water three times each.

Synthesis of azobenzene-modified SiO_2@CTAB/SiO_2 (SiO_2@CTAB/Azo-SiO_2)

The SiO_2@CTAB/Azo-SiO_2 was prepared according to the reported method with major modifications.[13] Firstly, the mixture of 4-PPA (0.284 g) and ICPES (1.42 mL) was dissolved in 10 mL ethanol and the mixture was refluxed under nitrogen for 4 h to obtain azobenzene-modified ICPES (Azo-ICPES). Secondly, the as-prepared SiO_2 (100 mg) was homogeneously dispersed in deionized water (20 mL) by ultrasonication for 30 min. The white suspension was then added to a mixture solution containing CTAB (150 mg), ethanol (30 mL), deionized water (30 mL), and ammonia solution (0.55 mL). Thirdly, TEOS

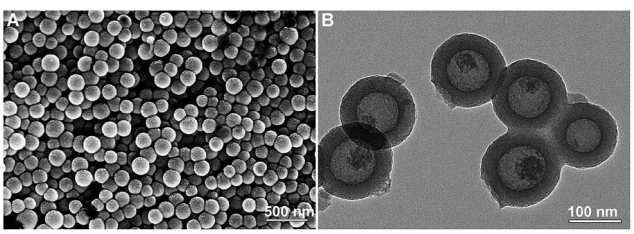

Fig. 1 (A) SEM and (B) TEM image of Azo-HMSs.

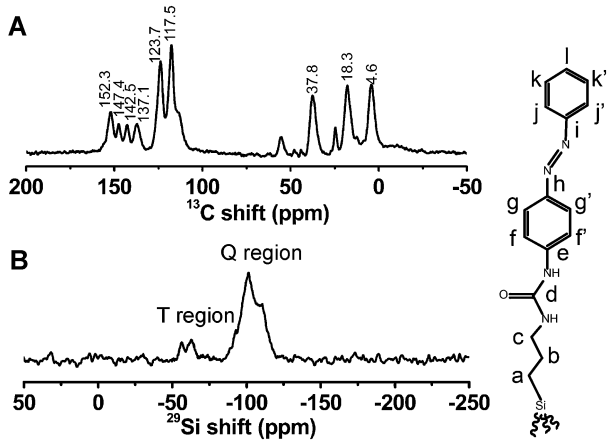

Fig. 2 (A) ^{13}C and (B) ^{29}Si CPMAS spectra of Azo-HMSs.

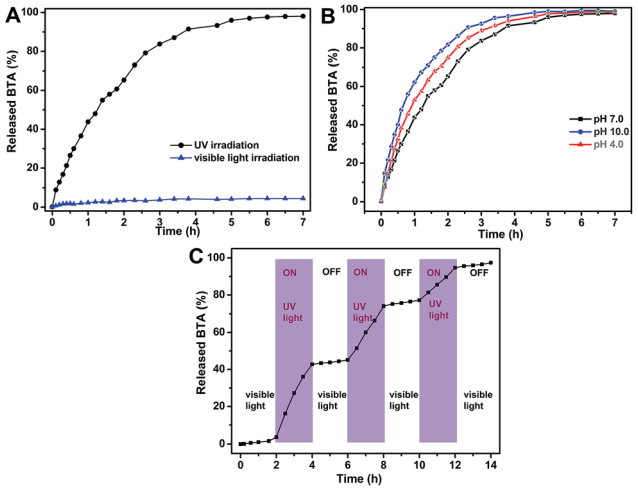

Fig. 3 (A) Time course of BTA release from Azo-HMSs under UV irradiation and visible light irradiation. (B) Release profiles of BTA from BTA@Azo-HMSs at pH 4.0, 7.0 and 10.0 under UV irradiation, respectively. (C) Photosensitive "on–off" release of BTA from BTA@Azo-HMSs as a function of time at different light wavelengths.

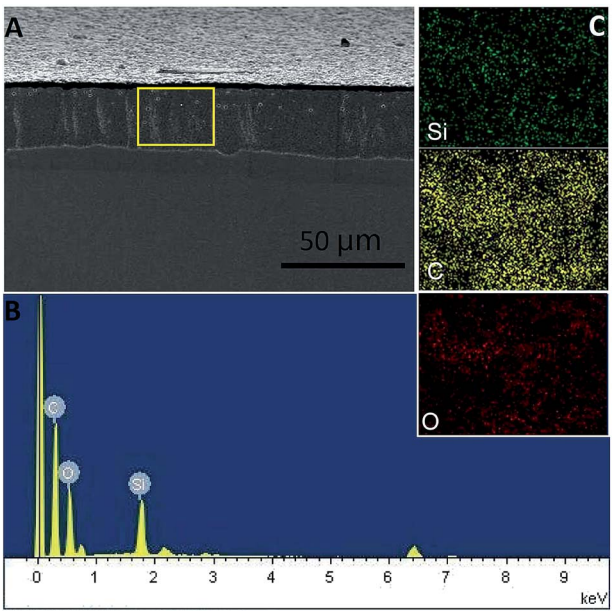

Fig. 4 (A) FE-SEM cross-section image and (B), (C) the corresponding elemental mapping (Si, O and C) of a selected area of the Azo-HMS doped alkyd coating.

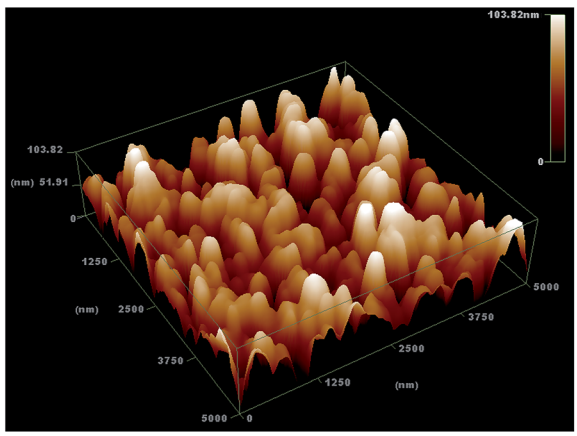

Fig. 5 AFM surface image of the Azo-HMS embedded alkyd coating.

(0.25 mL) and Azo-ICPES (0.25 mL) were slowly added after stirring at room temperature for 30 min. After the reaction was vigorously stirred for another 6 h, the yellow powder was extracted by centrifugation, and washed with ethanol and deionized water three times. Finally, the product was re-dispersed in 20 mL deionized water for the next step.

Synthesis of Azo-HMSs

The SiO_2@CTAB/Azo-SiO_2 solution was dispersed by ultrasonication for 20 min and stirred for 4 h. Sodium carbonate (470 mg) was dissolved into the above solution and stirred at 50 °C for 10 h to selectively etch the SiO_2 cores. The obtained Azo-HMS nanoparticles were collected by centrifugation and washed with water thoroughly. To completely remove the CTAB surfactant, the product was dispersed into methanol/HCl (50 mL/4 mL (37%), v/v) mixture solution and refluxed at 80 °C overnight. The Azo-HMSs were collected by centrifugation, rinsed with deionized water, and dried under vacuum.

Loading of corrosion inhibitors

Azo-HMSs (50 mg) were dispersed into 10 mg mL^{-1} solution of benzotriazole (BTA, 5 mL) and the mixture was placed in a hermetic vial. The air inside the vial was repeatedly evacuated using a vacuum pump (100 mbar for 10 min). After the bubbles disappeared, the dispersion was sealed in the vial and stirred for 4 h under UV irradiation ($\lambda = 360$ nm). The above procedure was repeated three times to maximize the adsorbed amount of BTA in the large hollow cavity of Azo-HMSs. The surface-adsorbed BTA was washed with deionized water and then the as-prepared BTA-loaded Azo-HMSs (BTA@Azo-HMSs) were

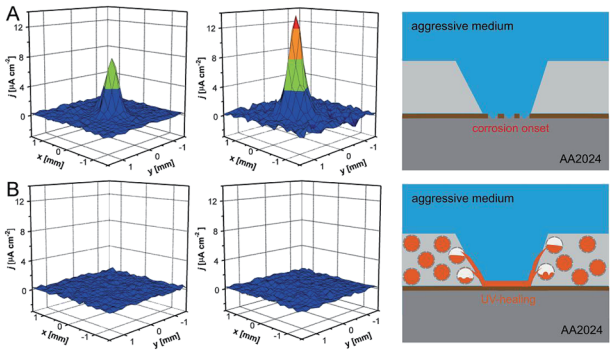

Fig. 6 SVET current density maps of aluminium coated with the alkyd coating without (A) and with (B) the BTA@Azo-HMSs nanocontainers obtained after 1 h (left column) and 10 h (middle column) immersion in 0.1 M NaCl. The passive protection performance of the pure coating and the active self-healing performance of the coating containing BTA@Azo-HMSs was compared when the scratches were exposed to the UV light (right column).

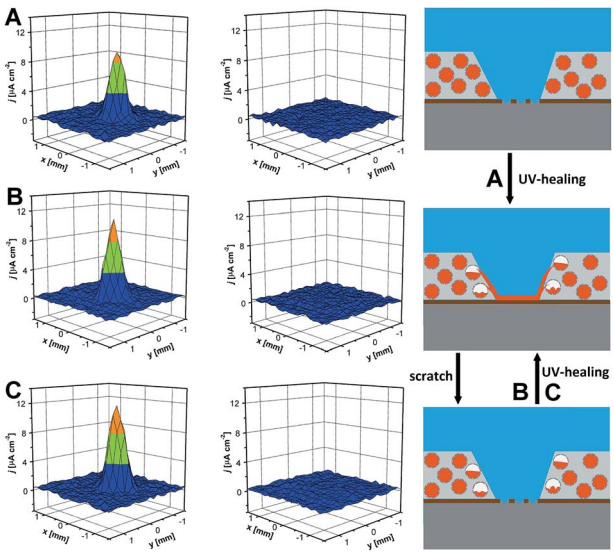

Fig. 7 (A) SVET current density maps of aluminium coated with the alkyd coating containing the nanocontainers after 2 h local UV irradiation upon the corrosion site. (B) SVET current density maps obtained after 2 h irradiation of local UV when the same position was scratched again. (C) SVET current density maps obtained by repeating the above operations.

separated by centrifugation at 10 000 rpm for 10 min and dried overnight at 50 °C under vacuum. All of the washing solutions were collected, and the loading amount of BTA was calculated according to the difference in the weight ratio of initial and residual BTA.

Light-activated controlled release

The BTA@Azo-HMSs (1 mg) were placed into a dialysis bag (MW 40 000), which was immersed into a cuvette containing 4 mL PBS solution (pH = 7). The released BTA could cross the dialysis membrane but not the nanoparticles. The Azo-HMS powder was

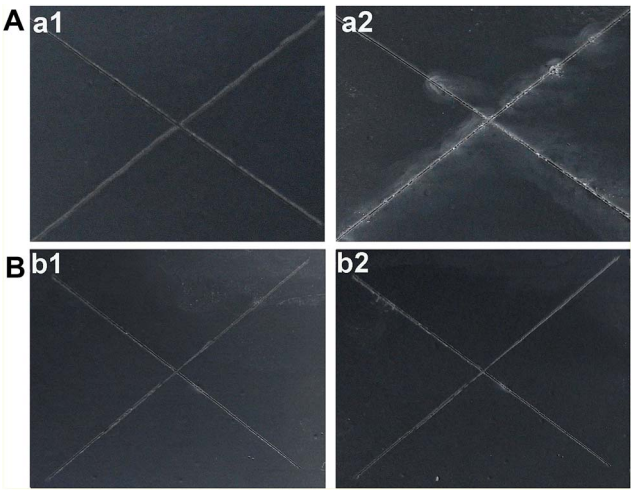

Fig. 8 Optical photographs of the scratches on aluminium substrate coated with (A) the pure alkyd coating and (B) the alkyd coating containing the BTA@Azo-HMSs nanocontainers, respectively, before (a1 and b1) and after (a2 and b2) immersion in a 0.1 M NaCl solution for 96 h under UV light.

irradiated with UV light (365 nm). During this period of time, UV-vis absorption spectra of the solution were recorded at predetermined time points.

The formation of anticorrosion coating

The aluminium plates (1 × 2 cm) used as the substrates for corrosion tests were pretreated as follows: (a) degreased in acetone; (b) immersed into a NaOH solution (1 M) at 60 °C for 15 min and rinsed with deionized water; (c) etched in a HNO_3 solution (15%) at 25 °C for 10 min and washed with water; (d) dried with a N_2 flow. BTA@Azo-HMSs were directly added into alkyd resins. To homogeneously disperse the nanocontainers, the samples were mixed using a rotor–stator stirrer for 4 h. Then the substrates were dipped into the resin for 90 s and withdrew at a speed of 12 cm min^{-1} using a PT MM01 dip-coater.

Characterizations

IR (Bruker Tensor 27 FTIR spectrometer), SEM (Hitachi S-4800), TEM (JEM-2100F), UV-vis spectroscopy (Shimadzu UV-1800 spectrometer), N_2 sorption (Quanta chrome Nova 1000 Micrometric apparatus), and the solid state ^{13}C and ^{29}Si CPMAS NMR spectrometer (Bruker DSX 400 NMR) were used to characterise the various samples. The self-healing performance of the alkyd coatings doped with nanocontainers was investigated by the scanning vibration electrode technique (M370 device, from Princeton Applied Research). Experimental details can be seen in a previous paper by our group.[4b]

Results and discussion

Preparation and characterizations of Azo-HMSs

The Azo-HMSs were prepared according to a combined strategy of bifunctional modification[14] and selective etching process (Scheme 2).[15] TEM images of uniform SiO_2 spheres and

SiO_2@CTAB/Azo-SiO_2 are shown in Fig. S1.† The TEM image in Fig. 1B reveals the Azo-HMSs with a hollow cavity diameter of 100 ± 5 nm and a mesoporous shell of 25 ± 2.5 nm. However, the mesoporous structure of Azo-HMSs cannot be clearly observed due to the successful grafting of azobenzene molecules in the mesoporous interiors. The FTIR spectrum (Fig. S2†) was utilized to verify the immobilization of azobenzene groups on the side walls of the mesopores.

Moreover, the UV-vis spectroscopy analysis (Fig. S3†) and CPMAS NMR (Fig. 3) revealed the successful grafting the azobenzene groups. In the solid-state ^{13}C NMR spectrum, the three signals at δ = 4.6, 18.3, and 37.8 ppm corresponded to the carbon atoms at the a, b and c positions of the silica surface, respectively. The peak at δ = 152.3 ppm corresponds to the d atom. The signals at δ = 117.5, 123.7, 137.1, 142.5, and 147.3 ppm corresponded to f/f′, g/g′/j/j′, k/k′/l, e, and h/i, respectively. N_2 sorption analysis of Azo-HMSs shows a type IV isotherm with a BET surface area of 991.1 $m^2\ g^{-1}$ and a total pore volume of 0.86 $cm^3\ g^{-1}$, and the BJH analysis exhibits a narrow pore size distribution centered at 2.1 nm (Fig. S4†). After encapsulating the hollow cavity with BTA molecules, a significant decrease of total pore volume to 0.35 $cm^3\ g^{-1}$ was observed, showing that the large cavity has been filled with BTA. Thus, the maximum loading capacity of Azo-HMSs for BTA molecules is about 25.2 wt% by analyzing the TGA data. The immobilization efficiency of azobenzene was calculated to be 0.2 mmol g^{-1} SiO_2 by TGA (Fig. S5†). Thus, the well-designed nanocontainers consist of interior cavities for high loading capacity of corrosion inhibitors and mesoporous side walls modified with light-responsive molecular switches can transport the inhibitor molecules in and out of the Azo-HMSs on demand.

Reversible and light-responsive release behavior

To investigate the photo-controlled release properties of BTA@Azo-HMSs, a solution of BTA@Azo-HMSs was then exposed to different wavelengths of light. The precise control of corrosion inhibitors was verified by monitoring the concentration of the released BTA after exposure to UV light and visible light. At first, the premature release of BTA@Azo-HMSs in aqueous neutral solutions was examined under visible light as shown in Fig. 3A. It should be noted that the hybrid can completely prevent the premature release without any additional capping operation. Since the *cis* isomer of the azobenzene molecules transforms into the *trans* isomer under visible light irradiation, they act as gatekeepers over the openings in nanopores to prevent the diffusion of the corrosion inhibitors into the solution. When the wavelength was changed to 365 nm, the amount of BTA leaked into the solution quantified by UV absorbance increases distinctly. No noticeable release of BTA (4.0%) was detected by UV-vis spectroscopy under neutral pH after 7 h, as well as under acidic or alkaline pH. In contrast, the *trans* form is converted to the *cis* form upon exposure to UV (365 nm), causing the leakage of corrosion inhibitors into the solution. The release amount of BTA in the neutral solution increased significantly, and 90% of BTA released was observed after 4 h. Furthermore, the release characteristics of Azo-HMSs were also studied in alkaline or acidic solutions, because every corrosion process is accompanied by the local acidification and local alkalization in the corrosion area. As shown in Fig. 2B, the release profiles in acidic and alkaline conditions are similar to that in neutral conditions. Interestingly, the release rate of BTA in acidic conditions is higher than for neutral conditions and the release rate is the highest in alkaline conditions. It is not difficult to understand that both the silica particles and BTA molecules have the same charge when pH values deviate heavily from the neutral value, resulting in larger electrostatic repulsion forces of each other and faster release. The rapid response and precise recognition capability of the azobenzene-based molecular switches make it possible to realize the desired photo-controlled release. These release characteristics are very suitable for the application of the light-sensitive nanocontainers in the active anticorrosion coatings. For smart coatings, the rapid release of active materials from the nanocontainers, which could be immediately activated by UV light, is a great advantage after the onset of perception of corrosion.

Another unique advantage of the Azo-HMSs lies in reversible molecular switches, which can achieve controlled release of BTA in a photosensitive "on–off" release pattern. As demonstrated in Fig. 3C, a distinct release of BTA occurred when the wavelength switched to 365 nm, and 42% release was obtained after 2 h irradiation of UV. The closed state of molecular switches completely constrained the diffusion of the BTA molecules under visible light for 2 h. Subsequent irradiation under UV for 2 h again made the diffusion of 30% of BTA from the pore cavities into the solution. It is concluded that the release profiles demonstrate that the "on–off" switching is reversible and can be repeatedly operated many times. On the basis of the reversible photosensitive azobenzene molecule switches, the "release–halt–release" behaviour of the BTA molecules from Azo-HMSs can be realized automatically *via* the sequential alternation of irradiation wavelengths. In general, the characteristics of the Azo-HMSs, such as high loading capacity, reversible light-responsive controlled release, zero release under neutral solution and fast release behavior under acidic and alkaline solutions can be utilized by smart nanocontainers to construct intelligent anticorrosion coatings.

Characterization of the anticorrosion coating

The water-based alkyd coating in this study was deposited on the aluminium alloy AA2024 by the dip-coating technique. Fig. 4 shows the cross-section SEM image of an Azo-HMS doped alkyd coating with a thickness of 25 μm. To illustrate the distribution of silica nanocontainers in the side view of the coating, an EDS spectrum and elemental mapping were obtained. The coating impregnated with the Azo-HMSs is mainly composed of silica, carbon and oxygen elements, as shown in Fig. 4. It is worth noting that the silicon element has a high peak and is evenly allocated in the alkyd coatings, due to the existence of the silica nanocontainers as the active component of the coating. The AFM analysis in Fig. 5 reveals the homogeneous distribution of single or several nanocontainers over the surface of the coating. The high surface concentration of the amount of nanocontainers is

$\sim 10^{10}$ per m^2, as estimated by the AFM image (Fig. 5). These results also demonstrated that the environmentally friendly water-based alkyd coating can provide excellent dispersibility for the light-responsive nanocontainers.

Continuous self-healing ability

To confirm the active anticorrosion performance provided by the light-sensitive nanocontainers, local current density measurements around the artificial scratches were performed by employing the scanning vibration electrode technique (SVET). The alkyd coatings were scratched with a sharp blade to expose the metal surface in order to activate the corrosion degradation in a 0.1 M NaCl aqueous solution. The scratches have a length of 2 mm and a width of $\sim$35 μm. The current density maps for aluminium alloy AA2024 coated with the coating without and with BTA@Azo-HMSs were depicted in Fig. 6 after 1 and 10 h of immersion in 0.1 M NaCl solution. An anodic current density maximum of 6.3 μA cm^{-2}, relating to the redox reaction between aluminium and the water oxygen, can be detected above the surface scratch of the pure coating after 1 h of immersion in 0.1 M NaCl solution (Fig. 6A). At the same time corrosion was not detected in the coating containing BTA@Azo-HMSs. However, after 10 h of immersion, a significant anodic peak of 13.4 μA cm^{-2} can be observed at the scratch area by exposure to local UV irradiation (Fig. 6A). On the contrary, the corrosion process in the alkyd coatings containing BTA@Azo-HMSs has been effectively suppressed, and the maximal current density remained constant at the noise level (Fig. 6B).

To verify the role of the reversible photo-controlled release system in the self-healing process, the SVET was also used to monitor the changing trends of local current density by switching of the UV and visible light. In the case of the coating containing BTA@Azo-HMSs, the anodic current density reached 8 μA cm^{-2} after 1 h immersion without UV irradiation. After 2 h of UV irradiation, a sufficient amount of BTA was released from the nanocontainers, which results in complete suppression of the corrosion at the site of the scratches, as evidenced by 3D current density maps (Fig. 7A). To demonstrate the reversible opening–closing behavior of Azo-HMS incorporation into the alkyd coating, the scanned site was carefully scratched again to accelerate the corrosion. Consequently, the current density increases to 10.8 μA cm^{-2} as shown in Fig. 7B, which reveals the occurrence of the corrosion process. Subsequently, it is clearly seen from Fig. 7B that the corrosion activity disappears after 2 h irradiation of UV, since the anodic current density is relatively low and close to the noise level. When repeating the same operation for the third time, an obvious anodic peak disappeared after UV irradiation for 2 h (Fig. 7C). However, for the fourth time, an anodic peak of 12 μA cm^{-2} could still be observed after UV irradiation (Fig. S6†). This can be interpreted as an insufficient amount of active molecules being released by the remote UV stimulus, so as not to prevent the propagation of corrosion in the scratch. Overall, the delicate design of a hollow structure for smart nanocontainers can provide enough corrosion inhibitors to suppress the corrosion reaction for improving the long-term performance of the metal. More interestingly, the anticorrosion coating by incorporating hollow nanocontainers with photoresponsive azobenzene molecular switches can also the avoid excessive release of active molecules after the corrosion healing and repair the same scratch more than once.

To evaluate the protection ability and stability of the coating, an aluminium substrate with scratches on the coating was immersed in a 0.1 M NaCl solution under UV irradiation. After 96 h, the corrosion products can be observed on the aluminium coated by the pure alkyd coating without nanocontainers after constant irradiation with UV light (Fig. 8A). In contrast, no notable corrosion products appeared on the scratch coated by the alkyd coating containing the BTA@Azo-HMS nanocontainers (Fig. 8B). The different results of control experiments confirmed the long-term anticorrosion ability and stability of the alkyd coating containing BTA@Azo-HMSs.

Conclusions

In summary, azobenzene-modified hollow mesoporous nanocontainers with reversible and light-responsive release properties have been prepared and successfully incorporated with alkyd coating onto aluminium substrates. The composite coating can automatically repair the corrosion area upon UV irradiation when scratched, due to the light and pH-stimulated release of corrosion inhibitors during the corrosion process. Additionally, the azobenzene-modified nanocontainers embedded into the coating can release corrosion inhibitors under UV irradiation, completely trap them upon visible light illumination, and release them again when exposed to UV light. Therefore, the concept of reversible photoresponsive release introduced here is able to provide long-time protection for underlying substrates even when the cured defect is damaged again.

Acknowledgements

This research was financially supported by the Thousand Young Talents Program of China, the Young Scientist Project of National Basic Research (973) Program of Ministry of Science and Technology of China (no. 2015CB659300) and the National Natural Science Foundation of China (no. 21403105). This work was also supported by a Project Funded by the Priority Academic Program Development of Jiangsu Higher Education Institutions (PAPD).

Notes and references

1 Z. Liu, P. H. Chong, A. N. Butt, P. Skeldon and G. E. Thompson, *Appl. Surf. Sci.*, 2005, **247**, 294.
2 W. J. Clark, J. D. Ramsey, R. L. McCreery and G. S. Frankel, *J. Electrochem. Soc.*, 2002, **149**, B179.
3 R. L. Twite and G. P. Bierwagen, *Prog. Org. Coat.*, 1998, **33**, 91.
4 (*a*) M. A. Jakab and J. R. Scully, *Nat. Mater.*, 2005, **4**, 667; (*b*) J. J. Fu, T. Chen, M. D. Wang, N. W. Yang, S. N. Li, Y. Wang and X. D. Liu, *ACS Nano*, 2013, **7**, 11397; (*c*) E. V. Skorb, D. Fix, D. V. Andreeva, H. Möhwald and D. G. Shchukin, *Adv. Funct. Mater.*, 2009, **19**, 2373; (*d*) Z. L. Zheng, X. Huang, M. Schenderlein, D. Borisova, R. Cao,

H. Möhwald and D. G. Shchukin, *Adv. Funct. Mater.*, 2013, **23**, 3307; (*e*) D. G. Shchukin, M. Zheludkevich, K. Yasakau, S. Lamaka, M. G. S. Ferreira and H. Möhwald, *Adv. Mater.*, 2006, **18**, 1672; (*f*) D. G. Shchukin and H. Möhwald, *Adv. Funct. Mater.*, 2007, **17**, 1451; (*g*) T. Chen and J. J. Fu, *Nanotechnology*, 2012, **23**, 505705; (*h*) H. G. Wei, Y. R. Wang, J. Guo, N. Z. Shen, D. W. Jiang, X. Zhang, X. R. Yan, J. H. Zhu, Q. Wang, L. Shao, H. F. Lin, S. Y. Wei and Z. H. Guo, *J. Mater. Chem. A*, 2015, **3**, 469; (*i*) G. L. Li, M. Schenderlein, Y. Men, H. Möhwald and D. G. Shchukin, *Adv. Mater. Interfaces*, 2014, **1**, 1300019.

5 G. L. Li, Z. L. Zheng, H. Möhwald and D. G. Shchukin, *ACS Nano*, 2013, **7**, 2470.

6 (*a*) E. V. Skorb, A. G. Skirtach, D. V. Sviridoc, D. G. Shchukin and H. Möhwald, *ACS Nano*, 2009, **3**, 1753; (*b*) E. V. Skorb, D. V. Sviridov, H. Möhwald and D. G. Shchukin, *Chem. Commun.*, 2009, **40**, 6041.

7 A. Vimalanandan, L. P. Lv, T. H. Tran, K. Landfester, D. Crespy and M. Rohwerder, *Adv. Mater.*, 2013, **25**, 6980.

8 J. Tedim, M. L. Zheludkevich, A. N. Salak, A. Lisenkov and M. G. S. Ferreira, *J. Mater. Chem.*, 2011, **21**, 15464.

9 (*a*) M. X. Han, R. Michel, B. He, Y. S. Chen, D. Stalke, M. John and G. H. Clever, *Angew. Chem., Int. Ed.*, 2013, **52**, 1319; (*b*) Q. Yuan, Y. F. Zhang, T. Chen, D. Q. Lu, Z. L. Zhao, X. B. Zhang, Z. X. Li, C. H. Yan and W. H. Tan, *ACS Nano*, 2012, **6**, 6337; (*c*) J. Lu, E. Choi, F. Tamanoi and J. I. Zink, *Small*, 2008, **4**, 421; (*d*) J. N. Liu, W. B. Bu, L. M. Pan and J. L. Shi, *Angew. Chem., Int. Ed.*, 2013, **52**, 4375.

10 (*a*) J. Garcia-Amorós, S. Nonell and D. Velasco, *Chem. Commun.*, 2012, **48**, 3421; (*b*) G. S. Kumar and D. C. Neckers, *Chem. Rev.*, 1989, **89**, 1915.

11 S. Angelos, E. Choi, F. Vogtle, L. D. Cola and J. I. Zink, *J. Phys. Chem. C*, 2007, **111**, 6589.

12 W. Stöber, A. Fink and E. Bohn, *J. Colloid Interface Sci.*, 1968, **26**, 62.

13 X. Fang, C. Chen, Z. Liu, P. Liu and N. F. Zheng, *Nanoscale*, 2011, **3**, 1632.

14 (*a*) P. N. Minoofar, B. S. Dunn and J. I. Zink, *J. Am. Chem. Soc.*, 2005, **127**, 2656; (*b*) P. N. Minoofar, R. Hernandez, S. Chia, B. Dunn, J. I. Zink and A. C. Franville, *J. Am. Chem. Soc.*, 2002, **124**, 14388.

15 Y. Chen, H. R. Chen, L. M. Guo, Q. J. He, F. Chen, J. Zhou, J. W. Feng and J. L. Shi, *ACS Nano*, 2010, **4**, 529.

